Neutron Diffraction Study of Distorted-Triangular-Lattice Ising-like Antiferromagnet TlCoCl$_3$

Yoichi Nishiwaki[*], Tetsuya Kato[1], Yasuaki Oohara[2], Akira Oosawa[3],
Norikazu Todoroki[4], Naoki Igawa[5], Yoshinobu Ishii[5] and Katsunori Iio

*Department of Physics, Graduate School of Science and Engineering, Tokyo Institute of Technology,
2-12-1 O-okayama, Meguro-ku, Tokyo 152-8551*
[1]*Faculty of Education, Chiba University, 1-33 Yayoi-cho, Inage-ku, Chiba 273-8522*
[2]*Neutron Science Laboratory, Institute for Solid State Physics, University of Tokyo,
106-1 Shirakata, Tokai, Ibaraki 319-1106*
[3]*Department of Physics, Sophia University, 7-1 Kioi-cho, Chiyoda-ku, Tokyo 102-8554*
[4]*Institute of Physics, Kanagawa University, 3-27-1 Rokkaku-bashi, Kanagawa-ku, Yokohama 221-8686*
[5]*Japan Atomic Energy Agency, Tokai, Ibaraki 319-1195*

A powder and single-crystal neutron diffraction study was performed on the structural and magnetic phase transitions of the distorted-triangular-lattice Ising-like antiferromagnet TlCoCl$_3$. From the results of powder sample measurement, the crystal structures were identified as the $P6_3cm$ and $Pbca$ structures at the intermediate-temperature ($75 < T < 165\,$K) and lowest-temperature ($T < 68\,$K) phases, respectively. From the results of single-crystal measurement, it was clarified that Ising spins were arranged in an up-up-down-down manner with a triple-domain formation below the Néel temperature. Satellite peaks on the shoulder of magnetic peaks were observed near the Néel temperature.

1. Introduction

Numerous studies have been carried out on many compounds with a CsNiCl$_3$-type crystal structure (space group symmetry $P6_3/mmc$), which exhibit a one-dimensional feature on a linear-chain substructure and a spin frustration originating from the antiferromagnetic interactions of a basal-plane triangular lattice.[1]

The CsNiCl$_3$-type compounds have a perovskite-like structure with hexagonally closely packed CsCl$_3$ layers, in which face-sharing NiCl$_6$ octahedra (*h-h-h* packing) run, forming a –NiCl$_3$– chain along the *c*-axis.[2] Their nearest-neighbor magnetic Ni^{2+} ions on the *c*-plane form an equilateral triangular lattice. The CsNiCl$_3$-type crystal structure is shown in Fig. 1(a). There are several compounds, such as KNiCl$_3$,[3–5] RbMnBr$_3$,[6–8] TlFeCl$_3$[9] and RbFeBr$_3$.[10] Their crystal structures are distorted from the prototype CsNiCl$_3$ structure through successive structural phase transitions. We call these compounds the members of the KNiCl$_3$ family. The lattice distortions of these compounds are characterized by the shifts of –BX$_3$– chains along the *c*-axis. The structural sequences of KNiCl$_3$-family compounds are shown in Fig. 2. Both phase I and II structures of KNiCl$_3$ are reported to be prototype CsNiCl$_3$-type structures. The phase I structure is characterized by the total disorder of the K$^+$ ion, which is observed only in KNiCl$_3$.[3] The phase III structure of KNiCl$_3$ is proposed as the $P6_3cm$ structure on the basis of the results of single-crystal X-ray and powder neutron diffraction measurements.[5] The phase V structure of RbMnBr$_3$ is proposed as an orthorhombic structure of the space group symmetry $Pbca$ on the basis of the results of single-crystal X-ray and neutron diffraction measurements.[8] The chain shifts of the
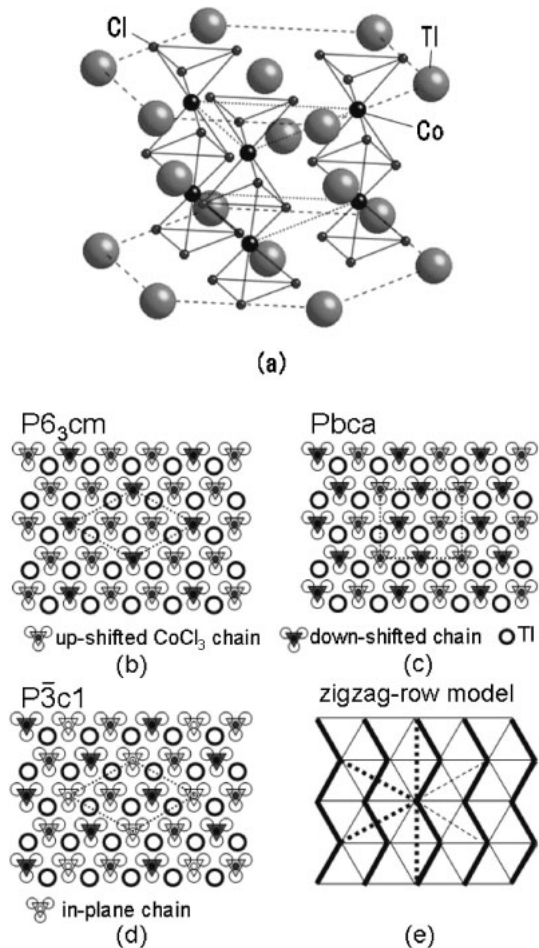

Fig. 1. (a) Prototype CsNiCl$_3$-type crystal structure. (b) Schematic drawing of shifts of CoCl$_3$ chains on $P6_3cm$ structure and (c) $Pbca$ and (d) $P\bar{3}c1$ structures. Drawings are projected on the *c*-plane. Broken lines show unit cells. (e) The magnetic interaction of the zigzag-row model corresponds to the $Pbca$ structure (c).

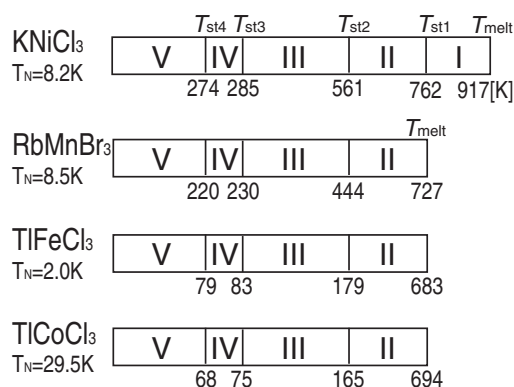*E-mail: nishiwaki@lee.phys.titech.ac.jp

Fig. 2. Structural phases of $KNiCl_3$-family compounds, $KNiCl_3$, $RbMnBr_3$, $TlFeCl_3$ and $TlCoCl_3$.

$P6_3cm$ and $Pbca$ structures are shown in Figs. 1(b) and 1(c), respectively. The chain shift of the $P6_3cm$ structure is arranged in an up-up-down manner in a unit cell and that of the $Pbca$ structure is arranged in an up-up-down-down manner in a unit cell. It is revealed by dielectric measurements that $TlCoCl_3$ undergoes structural phase transitions at $T_{st2} = 165$ K, $T_{st3} = 75$ K, and $T_{st4} = 68$ K.[11] Because $TlCoCl_3$ exhibits a similar gross temperature behavior of the dielectric constant to $KNiCl_3$, $RbMnBr_3$ and $TlFeCl_3$, its sequence of transitions must be identical with those of such compounds. Therefore, the lowest-temperature ($T < T_{st4}$) phase is expected to have an orthorhombic $Pbca$ structure.

These lattice distortions modulate the magnetic interaction. For XY spins, some models of triangular-lattice antiferromagnets with row, staggered-row and centered-honeycomb distortions have been investigated both theoretically and experimentally.[1,12] In addition, the zigzag-row distortion shown in Fig. 1(e) is also considered.[8] However, a similar study on Ising spin systems has been hardly carried out thus far. We are interested in studying the Co^{2+} Ising spin system on a distorted triangular lattice, because it is expected to show various types of magnetic ordering during the release of a strong spin frustration, even if the distortion is small.

For non distorted triangular-lattice antiferromagnets with Ising spins, extensive studies have been carried out on $CsCoCl_3$ and $CsCoBr_3$.[13–17] The strongest exchange interaction of these crystals is known to be the intrachain nearest-neighbor (NN) antiferromagnetic interaction J_0. Domain-wall solitons are propagated in a chain and the spins in the chain can be regarded as magnetic moments. These magnetic moments form a triangular lattice. Due to the spin frustration, these crystals undergo successive magnetic phase transitions. It is well known that a partial disorder (PD) phase appears at temperatures between the paramagnetic and ground states with ferrimagnetic (Ferri) spin arrangements. In the PD phase, the spins on one of the three sublattices on the c-plane are disordered and the spins on the other two sublattices are antiferromagnetically ordered. In order to explain those results, Mekata theoretically studied the magnetic phase diagram of the two-dimensional model using a mean-field approximation.[14] He introduced the interchain next-nearest-neighbor (NNN) ferromagnetic exchange interaction J_2 in addition to the interchain NN

antiferromagnetic J_1. For spin ordering, J_2 plays an important role as well as J_1, because this ferromagnetic J_2 connects identical sites and induces the spin ordering.

For distorted triangular-lattice antiferromagnets with Ising spins, we have already investigated one of such crystals, $RbCoBr_3$,[18–20] which is a unique $KNiCl_3$-family compound with Ising spins. $RbCoBr_3$ undergoes an antiferromagnetic phase transition at a structural phase transition temperature. The present compound $TlCoCl_3$ seems to be simpler because the magnetic phase transition ($T_N = 29.5$ K) occurs only far below the lowest structural phase transition (T_{st4}). Nevertheless, this magnetic ordering is interesting because Ising spins show a strong frustration on a distorted triangular lattice. Similar to that of $RbMnBr_3$, the magnetic interaction model of $TlCoCl_3$ is expected to be a zigzag-row one, as shown in Fig. 1(e). In the case of $RbCoBr_3$, the lattice is distorted according to the centered-honeycomb model. In the centered-honeycomb model, the ferromagnetic J_2 connects identical sites and induces the spin ordering. While in the case of the zigzag-row lattice, J_2 connects different sites because the unit cell changes to an orthorhombic one. Therefore, J_2 is also modulated as well as J_1. In Fig. 1(e), J_1 and J_2 are indicated as two (thick and thin) solid lines and two (thick and thin) broken lines, respectively. The ordered state of $TlCoCl_3$ is intriguing.

To investigate the lattice and spin structure, we performed the powder and single-crystal neutron diffraction measurements in $TlCoCl_3$. The crystal symmetries of phases III and V were identified as the $P6_3cm$ and $Pbca$ structures, respectively. The Ising spins of $TlCoCl_3$ were arranged in an up-up-down-down manner with a triple-domain formation.

2. Experimental Procedures and Results

2.1 Powder sample

The single crystals of $TlCoCl_3$ were prepared by the vertical Bridgman technique using a melt of an equimolar mixture of $TlCl$ and $CoCl_2$ in evacuated quartz ampoules. The furnace temperature was maintained at $900\,°C$ until the sample was lowered at a rate of 3 mm/hour. Powder neutron diffraction measurements were carried out using a high resolution powder diffractometer (HRPD) at JRR-3M in the Japan Atomic Energy Agency (JAEA), Tokai.

The powder neutron diffraction patterns are shown in Figs. 3(a)–3(c), measured at room temperature (phase II), 90 K (phase III) and 50 K (phase V), respectively. These results indicated that small superlattice reflections were caused by structural phase transitions and that atom positions did not show major changes. We attempted Rietveld analyses using a structural model the same as that of $RbMnBr_3$, because the sequence of structural phase transitions of $TlCoCl_3$ was identical with that of $RbMnBr_3$, as shown in Fig. 2. The Rietveld analyses were carried out using the program RIETAN-2000.[21]

The scattering data of phases II, III, and V were well fitted to the models with the space groups $P6_3/mmc$ [Fig. 1(a)], $P6_3cm$ [Fig. 1(b)] and $Pbca$ [Fig. 1(c)], respectively. The obtained parameters are listed in Tables I, II and III with typical refinement factors: the reliable factor of pattern R_p, weighted one of pattern R_{wp}, expected one R_e and "goodness-of-fit" indicator S (= R_{wp}/R_e). For phase III, another
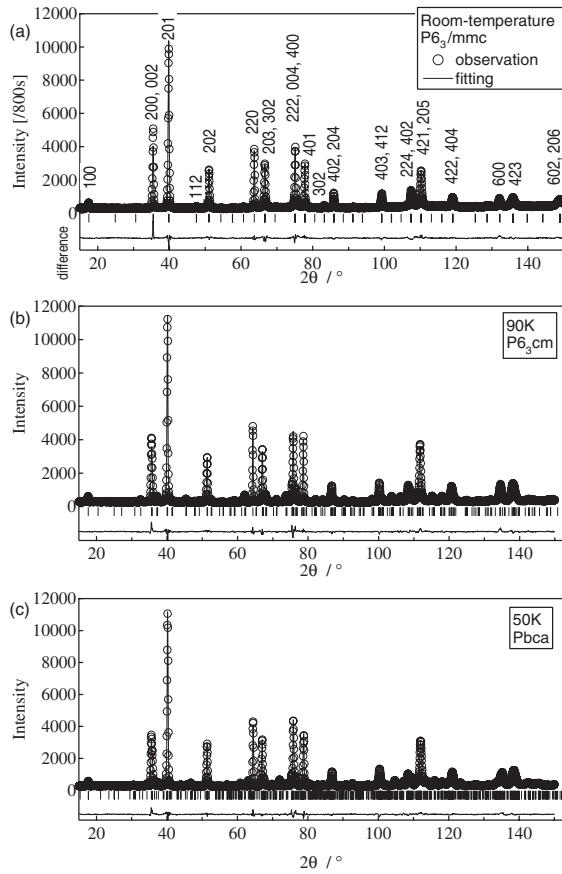
Fig. 3. Profiles of powder neutron diffraction. (a) Room temperature, (b) 90 K and (c) 50 K. The index (hkl) obtained using the prototype lattice is written in (a). Fitting lines are obtained using the program RIETAN-2000.[21] Fitting parameters are shown in Tables I–III.

Table I. Fitting parameters at room temperature by space group $P6_3/mmc$. U is the isotropic displacement parameter. The lattice constants are $a = 6.91$ Å and $c = 5.98$ Å. The refinement factors are $R_p = 5.17$, $R_{wp} = 6.90$, $R_e = 4.57$, and $S = 1.51$.

	x	y	z	$U/Å^2$
Tl	1/3	2/3	1/4	0.0451
Co	0	0	0	0.0365
Cl	0.3260	0.1630	1/4	0.0325

Table II. Fitting parameters at 90 K by space group $P6_3cm$. The lattice constants are $a = 11.86$ Å ($= \sqrt{3} \times 6.85$ Å) and $c = 5.96$ Å. The refinement factors are $R_p = 4.99$, $R_{wp} = 6.64$, $R_e = 4.59$, and $S = 1.45$.

	x	y	z	$U/Å^2$
Tl	0.6668	0	1/4	0.0189
Co	0	0	−0.0374	0.0076
Co	1/3	2/3	0.0372	0.0076
Cl	0.1630	0	0.2131	0.0109
Cl	0.3335	0.8297	0.2866	0.0109

model with the space group $P\bar{3}c1$ [Fig. 1(d)] produced almost the same reflections as the present $P6_3cm$ model. Here, the chain shift of the $P\bar{3}c1$ structure is arranged in an up-0-down manner. We also obtained the well-fitted parameters using the $P\bar{3}c1$ model for phase III, as shown in Table IV. The $P6_3cm$ structure does not have an inversion

Table III. Fitting parameters at 50 K by space group $Pbca$. The lattice constants are $a = 13.65$ Å ($= 2 \times 6.83$ Å), $b = 11.85$ Å ($= \sqrt{3} \times 6.84$ Å) and $c = 5.97$ Å. The refinement factors are $R_p = 4.45$, $R_{wp} = 5.85$, $R_e = 4.58$, and $S = 1.28$.

	x	y	z	$U/Å^2$
Tl	0.3769	0.4187	1/4	0.0099
Co	0.1274	0.2508	0.0447	0.0185
Cl	0.0009	0.1699	0.2939	0.0056
Cl	0.2469	0.1689	0.2985	0.0056
Cl	0.1260	0.4129	0.2895	0.0056

Table IV. Fitting parameters at 90 K by space group $P\bar{3}c1$. The lattice constants are $a = 11.86$ Å and $c = 5.96$ Å. The refinement factors are $R_p = 4.95$, $R_{wp} = 6.61$, $R_e = 4.59$, and $S = 1.44$.

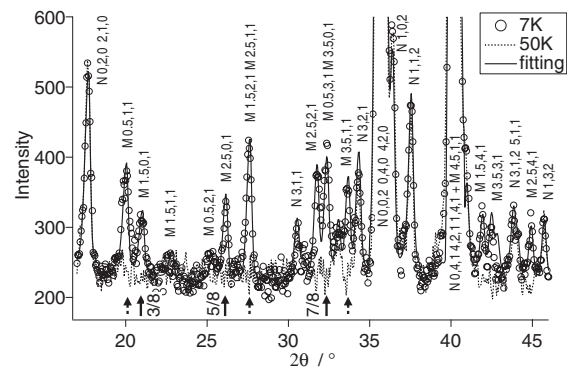|	x	y	z	$U/Å^2$
Tl	0.6678	0	1/4	0.0153
Co	0	0	0	0.0201
Co	1/3	2/3	−0.0452	0.0201
Cl	0.1630	0	1/4	0.0114
Cl	0.3332	0.8292	0.2068	0.0114

Fig. 4. Diffraction patterns of powder sample at 7 K (circle) and 50 K (dashed line). The nuclear (N) and magnetic (M) peaks are assigned with the h, k and l indices of the $2 \times \sqrt{3} \times 1$ orthorhombic lattice. Arrows with the solid and broken lines show the peak positions of on-plane and off-plane scatterings in the single-crystal measurements, corresponding to the circles and triangles in Fig. 5, respectively. The solid line is the fitting line obtained by using the program RIETAN-2000.[21] Here, we use the up-up-down-down spin structure described later [Fig. 9(a)].

center, while the $P\bar{3}c1$ structure has an inversion center. Although the spontaneous polarization of phase III of TlCoCl$_3$ was not clearly observed,[11] we adopted the $P6_3cm$ structure for phase III because the significant advantage of fitting was obtained in an additional single-crystal X-ray diffraction study.[22] Accordingly, in both phases III and V, similar amounts of displacements along the c-axes of Co and Cl from the prototype structures, z(Co) and z(Cl)–0.25, were obtained. Therefore, it was expected that each CoCl$_3$ chain would be shifted slightly along the c-axis while keeping the prototype shape in both phases III and V.

Figure 4 shows the powder pattern at 7 K. By comparing with the 50 K data (dashed line), the magnetic peaks were identified and assigned with indices $(hkl)^{or}$ (h = half-integer, k = integer and l = odd integer), which were described using the orthorhombic lattice. We attributed the absence of

$l =$ even peaks of the magnetic reflection to the antiferromagnetic ordering along the c-axis. The spin structure had a double period of the crystal unit cell along the a-axis.

2.2 Single crystal

For single-crystal measurements, neutron scattering was performed on the triple-axis spectrometer HQR installed at JRR-3M in JAEA. The spectrometer was used in the double-axis mode. A pyrolytic graphite (002) reflection was used for the monochromator. Higher-order neutrons were removed using the pyrolytic graphite filter set before the sample. The neutron energy was fixed at 13.6 meV ($k_{in} = 2.56$ rad/Å). Horizontal collimations were chosen as $20'$-$20'$-$60'$. The sample was about $0.5\,cm^3$ in volume. The sample was mounted in a refrigerator, and the temperature of the sample was measured with a calibrated silicon diode thermometer.

In the lowest-temperature phase, a triple-domain formation of orthorhombic lattices occurs, as shown in Fig. 5, as in the case of RbMnBr$_3$,[8] because the hexagonal in-c-plane symmetry is broken. However, for the sake of convenience, in the following description of the experimental conditions, we use the room-temperature CsNiCl$_3$-type lattice unless otherwise noted. The room-temperature unit cell is $a \times a \times c$ in real space, and the reciprocal points are described as (hkl). Accordingly, the lattice constants are $a = 6.83$ Å and $c = 5.93$ Å at $T = 4$ K. The sample was mounted with the [1$\bar{1}$0] axis arranged vertically so as to measure the scattering in the (h, h, l) zone. The unit cell of phase V is $2a \times \sqrt{3}a \times c$ in real space. The orthorhombic description will be explicitly shown as $(hkl)^{or}$, which is equivalent to $(2(h+k) - h + kl)$ for one orthorhombic domain.

We confirmed the consistency of the above-mentioned results with the powder sample data. The unit cell was enlarged $\sqrt{3} \times \sqrt{3} \times 1$ times below T_{st2}, and the lattice was distorted to an orthorhombic one below T_{st4}. The profile around the characteristic $(1/3, 1/3, 2)$ and $(1/4, 1/4, 2)$ peaks at 90 K (phase III), 70 K (phase IV) and 50 K (phase V) is shown in Fig. 6(a). The $(1/3, 1/3, 2)$ peak, which was prominent at 90 K, disappeared at 50 K, while the $(1/4, 1/4, 2)$ peak appeared. At 70 K, both the $(1/3, 1/3, 2)$ and $(1/4,$
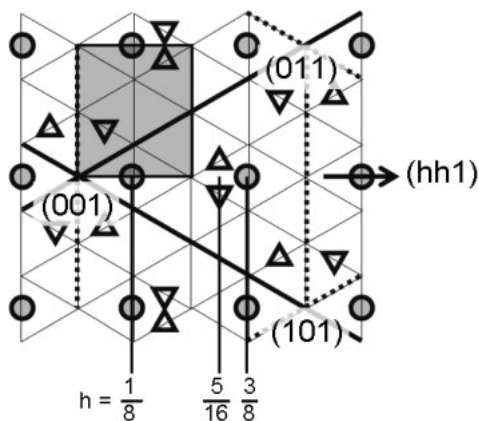

Fig. 5. Triple-domain formation in reciprocal space on ($hk1$) plane at lowest temperature. The circles indicate the reflections from one domain. The other domain contributions are shown by the upward and downward triangles. The phase V unit cell of one domain is shown by a rectangle. $h = 1/8$, $5/16$, and $3/8$ denote the observed positions on the ($hh1$) lines in the single-crystal measurment described in the text.
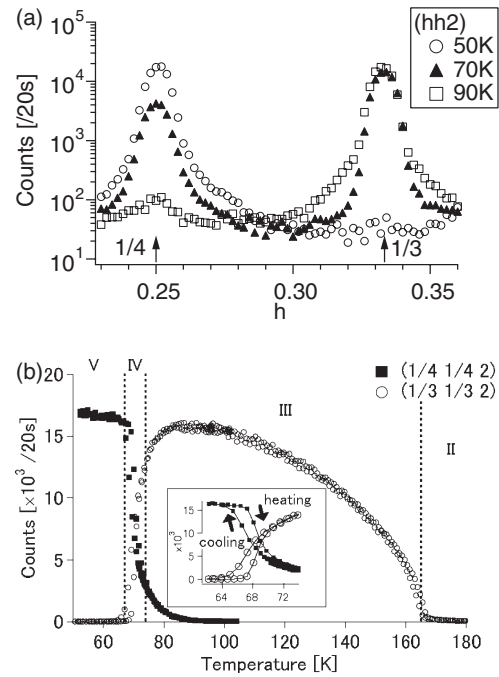

Fig. 6. (a) ($hh2$) profile at around $(1/4, 1/4, 2)$ and $(1/3, 1/3, 2)$. (b) Temperature dependences of $(1/4, 1/4, 2)$ and $(1/3, 1/3, 2)$ peak heights. The inset shows those at around T_{st3} (between phases III and IV) and T_{st4} (between phases IV and V).

$1/4, 2)$ peaks coexisted. We performed additional measurements of such profiles at several temperatures between 66 K and 84 K, but only the changes in the intensities of these peaks were observed. The shift of peak positions or the appearance of a peak with a different wave number was not observed. Figure 6(b) shows the $(1/3, 1/3, 2)$ and $(1/4, 1/4, 2)$ peak heights as a function of temperature. A thermal hysteresis was observed at around T_{st4} (between phases IV and V); thus, the transition at T_{st4} was of the first order. These results were consistent with these of dielectric measurements.[11]

The q-scan profiles of ($hh1$) and ($hh3$) at 4 K were obtained, as shown in Fig. 7. As indicated by the results of the powder sample measurement, $l =$ odd reflections were attributed to the magnetic reflection due to the antiferromagnetic ordering along the c-axis. The reflections $h = 1/8$, $5/16, 3/8$ and so on were observed. The gross results were similar to that of RbMnBr$_3$ under the magnetic field $H = 4.5$ T.[8] These peaks could be indexed using the orthorhombic lattice as $(1/8, 1/8, 1) = (1/2, 0, 1)^{or}$ and $(3/8, 3/8, 1) = (3/2, 0, 1)^{or}$. The $(5/16, 5/16, 1)$ peak corresponded to $(1/2, 1, 1)^{or}$ of two other domains, as shown in Fig. 5, which should be off-plane reflections because the vertical resolution of the present measurement might enable their detection. Small $h = 1/16$ and $15/16$ peaks also corresponded to the reflections of other domains. Thus, we concluded that the spin structure had a double period along the a-axis, which was consistent with the results of powder measurements.

However, the $(0, 0, l)$, $(1, 1, l)$, $(1/4, 1/4, l)$ and $(3/4, 3/4, l)$ ($l = 1, 3$) peaks, which were not observed on RbMnBr$_3$, appeared. These peaks were nuclear reflections because they did not disappear above T_N. The $(0, 0, l)$, $(1, 1, l)$ peaks could be attributed to the (002) and (222) reflections of the $\lambda/2$
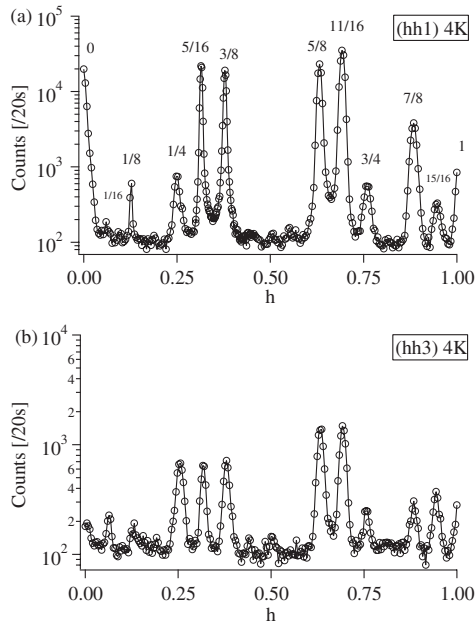
Fig. 7.   Neutron diffraction intensities of single-crystal TlCoCl$_3$ scanned parallel to ($hh1$) and ($hh3$) directions at 4 K.

neutron; however, the $(1/4, 1/4, 1)$ and $(3/4, 3/4, 1)$ peaks should be intrinsic reflections. The symmetry might be lower than $Pbca$, and the structural $Pbca$ model was valid as an approximate structure of phase V of TlCoCl$_3$.

It was confirmed that the spins were ordered at $T_N = 29.5$ K by magnetic susceptibility measurement.[11] Figure 8(a) shows the temperature variation of the profile at around $(3/8, 3/8, 1)$. We confirmed that the peak contained a diffuse scattering or small nuclear contribution because a small peak remained above T_N. Figure 8(d) shows the temperature dependence of the $(3/8, 3/8, 1)$ peak height. The peak height was saturated at about 22 K. It rapidly increased compared with the results for CsCoCl$_3$,[14] CsCoBr$_3$,[17] and RbCoBr$_3$.[20] Although another magnetic transition has been revealed to occur at 15 K by the magnetic susceptibility measurement of TlCoCl$_3$,[11] the present results showed no anomaly in the temperature dependence of the $(3/8, 3/8, 1)$ peak height at around 15 K. Moreover, the q-scan profiles of ($hh1$) and ($hh3$) at 20 K were entirely in accordance with those at 4 K. Above T_N, the diffuse scattering centering at around $(1/3, 1/3, 1)$ and $(2/3, 2/3, 1)$ was observed, as in the case of RbMnBr$_3$.[8] Immediately above T_N (only from about 30.0 to 29.5 K), additional satellite peaks appeared on the shoulder of the $(3/8, 3/8, 1)$ and $(5/8, 5/8, 1)$ peaks, as shown in Figs. 8(b) and 8(c). Their intensities and the center positions of wave number gradually changed with the temperature variation.

3.   Discussion

The phase IV structure of other KNiCl$_3$-family crystals has not been clarified thus far. The determination of the structure of this phase is important in elucidating the mechanism of lattice deformation from hexagonal phase III to orthorhombic phase V. The present results for TlCoCl$_3$ showed that the phase III reflection at $(1/3, 1/3, 2)$ and phase V reflection at $(1/4, 1/4, 2)$ coexisted. This indicates that phase IV seems to be a crossover from phase III to
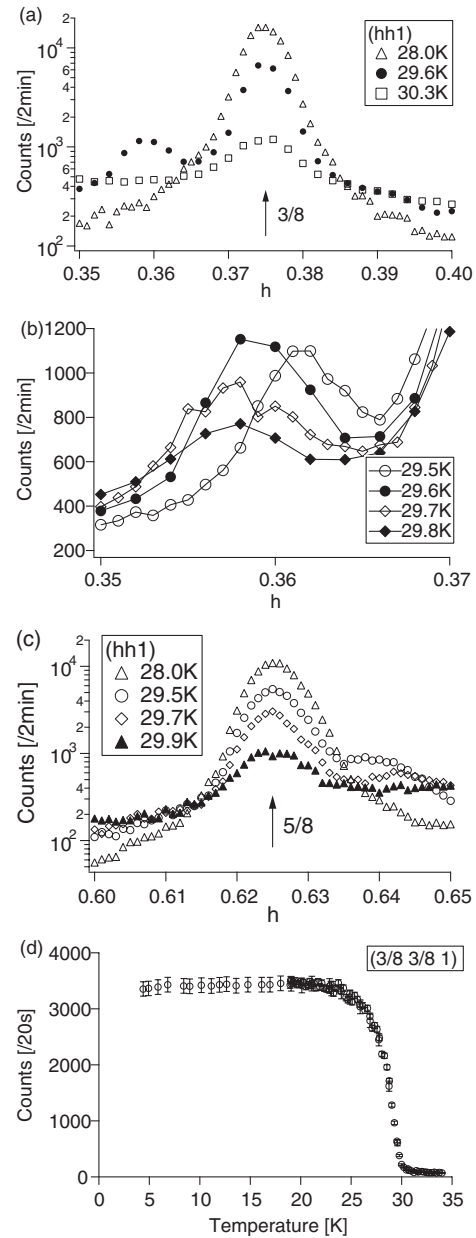

Fig. 8.   (a) ($hh1$) profile at around $(3/8, 3/8, 1)$. (b) Additional peak on shoulder of $(3/8, 3/8, 1)$ peak. (c) ($hh1$) profile at around $(5/8, 5/8, 1)$. (d) Temperature dependence of $(3/8, 3/8, 1)$ peak heights.

phase V, although the results of the dielectric and optical measurements indicate clear anomalies at T_{st3} (III ↔ IV) and T_{st4} (IV ↔ V). A further study is required.

Here, we discuss the spin structure in further detail, comparing the calculated intensities of some models with the data of the single-crystal measurements. As shown in the previous section, the magnetic unit cell had a double period along the a-axis, and the magnetic reflection appeared at $(n/8, n/8, l)$ ($n, l =$ odd integers) as indexed using the room-temperature lattice ($a \times a \times c$), which corresponds to $(n/2, 0, l)^{or}$ ($n, l =$ odd integers) as indexed using the lowest-temperature orthorhombic lattice ($2a \times \sqrt{3}a \times c$). In the following, we will describe the room-temperature lattice as $a_0 \times a_0 \times c_0$ and use the magnetic unit cell $a \times b \times c = 4a_0 \times \sqrt{3}a_0 \times c_0$, thus, the reflection indices are indicated as $(h^{mag}, 0, l^{mag})$ ($h^{mag}, l^{mag} =$ odd integers). For simplicity, the superscript^{mag} is omitted.

In our case, the reflections are observed only at $\mathbf{Q} = (h0l)$ so that the integrated intensity correlated by the Lorentz factor $I(\mathbf{Q})$ shows following $\mathbf{Q}$ dependence,[24)]

$$I(\mathbf{Q}) \propto f(\mathbf{Q})^2 \sum_{\alpha=x,y,z} \{1 - (\tilde{Q}_\alpha)^2\}\langle(S_\alpha(\mathbf{Q}))^2\rangle, \qquad (1)$$

where $f(\mathbf{Q})$ is the magnetic form factor of Co^{2+},[23)] $\tilde{Q}_\alpha = Q_\alpha/|\mathbf{Q}|$, $\mathbf{S}(\mathbf{Q}) = \sum_i \mathbf{S}_i \exp(i\mathbf{Q} \cdot \mathbf{r}_i)$ and $\langle\cdots\rangle$ denotes domain-averaged value. Because $ACoX_3$ compounds have an Ising spin system,

$$I(\mathbf{Q}) \propto f(\mathbf{Q})^2(1 - \tilde{Q}_z^2)\langle(S_z(\mathbf{Q}))^2\rangle$$

$$= f(\mathbf{Q})^2 \frac{\left(\frac{h}{a}\right)^2}{\left(\frac{h}{a}\right)^2 + \left(\frac{l}{c}\right)^2} \langle(S_z(\mathbf{Q}))^2\rangle. \qquad (2)$$

Now, we define the positions of 16 spins in the magnetic unit cell as

$$S_1 : \left(\frac{1}{16}, \frac{1}{4}, +\delta\right), \ S_2 : \left(\frac{3}{16}, \frac{3}{4}, +\delta\right),$$

$$S_3 : \left(\frac{5}{16}, \frac{1}{4}, -\delta\right), \ S_4 : \left(\frac{7}{16}, \frac{3}{4}, -\delta\right), \qquad (3)$$

and the other spins S_{4+i} ($i = 1, 2, 3, 4$) locate at $(x_{4+i}, y_{4+i}, z_{4+i}) = (x_i + \frac{1}{2}, y_i, z_i)$ and S_{8+i} ($i = 1, 2, \ldots, 8$) at $(x_{8+i}, y_{8+i}, z_{8+i}) = (x_i, y_i, z_i + \frac{1}{2})$, where the amounts of the up and down shifts of spins along the c-axis are expressed as δ. Two approximations, $0.1274 \sim 1/8$ and $0.2508 \sim 1/4$, are applied to the x- and y-coordinates of Co in Table III. The magnetic interaction along the c-axis is strongly antiferromagnetic; thus, S_{8+i} is antiparallel to S_i ($i = 1, 2, \ldots, 8$). Therefore,

$$S_z(\mathbf{Q}) = (1 - e^{i\pi l})\{(S_1 + e^{i\pi h}S_5)\alpha^h\beta^l$$
$$+ (S_2 + e^{i\pi h}S_6)\alpha^{3h}\beta^l$$
$$- (S_3 + e^{i\pi h}S_7)\alpha^{-3h}\beta^{-l}$$
$$- (S_4 + e^{i\pi h}S_8)\alpha^{-h}\beta^{-l}\}, \qquad (4)$$

where $\alpha = e^{i\pi/8}$ and $\beta = e^{i2\pi\delta}$. This reproduces the condition that the magnetic reflection is not observed at $l = $ even. Additionally, from the experiments, the intensities of the reflections at $h = $ even and $l = $ odd are also zero. Thus, it is appropriate to introduce a set of $S_{4+i} = -S_i$ ($i = 1, 2, 3, 4$) conditions, because the above formula changes to

$$S_z(\mathbf{Q}) = (1 - e^{i\pi l})(1 - e^{i\pi h})\{S_1\alpha^h\beta^l + S_2\alpha^{3h}\beta^l$$
$$- S_3\alpha^{-3h}\beta^{-l} - S_4\alpha^{-h}\beta^{-l}\}. \qquad (5)$$

For $h, l = $ odd integers, the factor $(1 - e^{i\pi l})(1 - e^{i\pi h})$ should be read as 4.

If full spin moments are grown at low temperatures, under the $S_{4+i} = -S_i$ condition, the spins along the a-axes S_1, S_3, S_5, and S_7 are arranged in an up-up-down-down manner whether $S_3 = S_1$ or $S_3 = -S_1$, as shown in Fig. 9(a). If there are sites on which full spin moments are not grown, for example disordered sites in an extreme case, the spins along the a-axis are arranged in an up-0-down-0 manner, as shown in Fig. 9(b). Similar discussions can be applied to the cases of S_2, S_4, S_6 and S_8. With these spin structures in mind, we performed least-squares fitting, using the intensity data
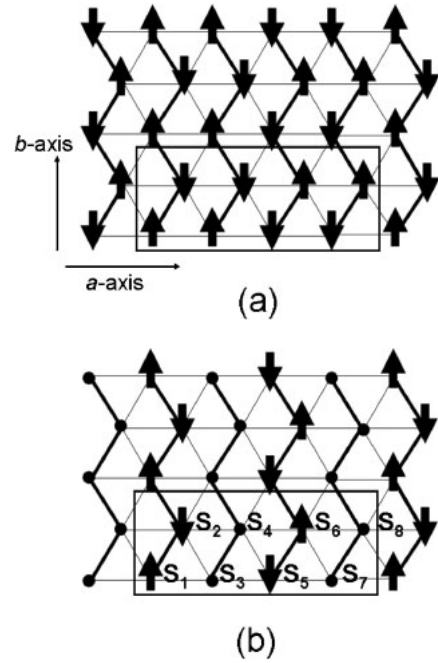

Fig. 9. Schematic configuration of Ising spins on zigzag-row lattice: (a) up-up-down-down and (b) up-0-down-0 structures. The black circles show disordered spins. The magnetic unit cell is also shown.

obtained at 4 K for 14 $h, l = $ odd magnetic and several nuclear peaks. We regarded the data at 35 K as the background diffraction. We could confirm the proportionalities of the $\tilde{Q}_z^2$ dependence of the corrected intensity $I' = I(\mathbf{Q})/f(\mathbf{Q})^2$, as shown in Figs. 10(a) and 10(b). From eq. (1), these proportionalities consist of Ising spins. Thus, the contribution from the transverse components of the spins is too small to be detected in the present measurements.[24)] In addition, the coefficient $|\hat{Q}_z|^2$ is found to have only two values of all (h, l) reflections. Thus, the formula $S_z(\mathbf{Q})$ in eq. (5) can be more simplified in practice. We consider that the chain shift ($\delta = 0.045$) slightly affects on the intensity because we should take the average of two domain structures $\delta = \pm 0.045$, in addition to the reasonable hypothesis $S_1 = \pm S_4$. Then, the fitting produced $S_{uudd} = 2.7 \ \mu_B$ for $S_1 = -S_2 = S_3 = -S_4 = S_{uudd}$ and $S_1 = -S_2 = -S_3 = S_4 = S_{uudd}$. The observed value I_{obs} vs calculated value I_{cal} plot is shown in Fig. 10(c), indicating that the spins are arranged in an antiferromagnetic manner along the zigzag chain direction b-axis, as shown in Fig. 9(a). On the other hand, an up-0-down-0 model, with $S_1 = -S_2 = S_{u0d0}$ and $S_3 = S_4 = 0$ [Fig. 9(b)], or $S_1 = S_4 = S_{u0d0}$ and $S_2 = S_3 = 0$, produced the same fitting results at the different intensities of the magnetic moment $S_{u0d0} = 3.8 \ \mu_B = \sqrt{2}S_{uudd}$. The Co^{2+} spin moments in $CsCoCl_3$,[14)] $CsCoBr_3$[17)] and $RbCoBr_3$[20)] range about from 2.5 μ_B to 3 μ_B; therefore, the up-up-down-down structure is reasonable. Additionally, because there is only one Co site in the *Pbca* structure as shown in Table III, the up-0-down-0 model might be impractical. Accordingly, we conclude that the ground state of the spin structure of $TlCoCl_3$ is the up-up-down-down structure.

We tried to obtain the calculated powder diffraction pattern when the spin structure was the up-up-down-down structure, using the program RIETAN-2000.[21)] The result at 7 K is shown in Fig. 4.
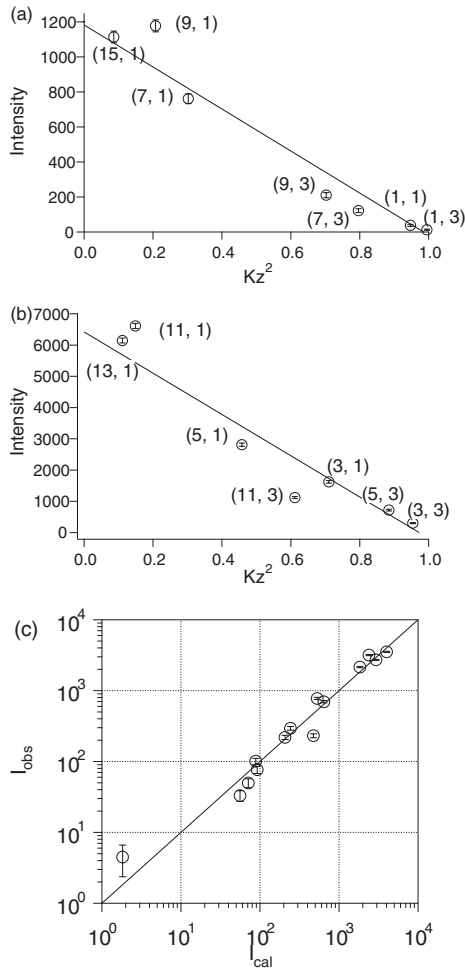
Fig. 10. $\tilde{\kappa}_z^2$ dependences of intensities of magnetic Bragg peaks (a) when $h^{\mathrm{mag}} = 1, 7, 9$, and 15, and (b) when $h^{\mathrm{mag}} = 3, 5, 11$, and 13. Here, the intensities are compensated by the magnetic form factor and Lorentz factor. The notation on the graph corresponds to (h^{mag}, l). (c) Observed value I_{obs} (vertical axis) vs calculated value I_{cal} (transverse axis).

Moreover, the satellite peaks appeared on the shoulder of the magnetic peaks immediately above T_{N}. The magnitudes of the spin moments of the up-up-down-down structure might be modulated around T_{N}. We propose a possible mechanism for the spin ordering of TlCoCl$_3$, using the axial next-nearest-neighbor Ising (ANNNI)-like frustrated model.[25] As well-known, the ANNNI model describes the change in the periodicity of the frustrated stacking of layered structures. The stacking periodicity changes with temperature in the presence of the frustration between the NN and NNN inter-plane interactions.

The present results show the change in periodicity along the a-axis. The exchange interaction J_1'' along the thick zigzag rows in Fig. 11(a) is expected to be stronger than that of the thin lines (J_1'), because the thick lines connect spins shifting in the same direction along the c-axis. We assume that the development of the magnetic correlation on the c-plane is anisotropic: only the correlation along the thick lines immediately develops at around T_{N}. The antiferromagnetic ordering along the zigzag rows should produce two possible structures, namely, the -up-down-up-down- and -down-up-down-up- structures. For this freedom, we can put the 'pseudo-spins' $S = \pm 1$ on the zigzag rows, as shown in Fig. 11(a).
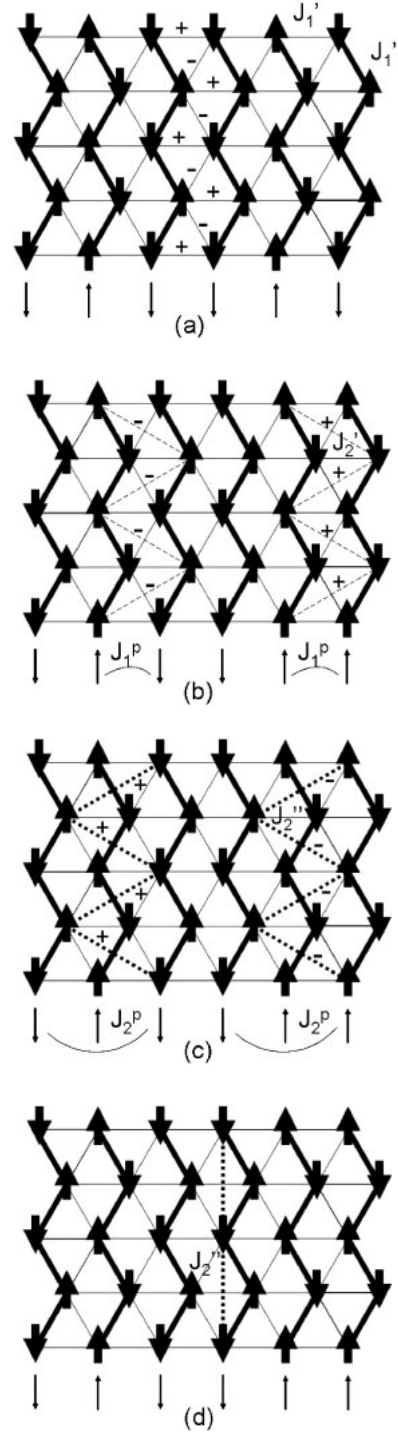

Fig. 11. (a) The NN interactions J_1' between real spins are canceled out. '+' denotes the bond that increases the energy. '−' denotes the bond that decreases the energy. (b) The ferromagnetic NNN interactions between real spins, J_2', affect the antiferromagnetic NN interactions J_1^{p} between pseudo-spins. (c) Another J_2'' affects the antiferromagnetic NNN interactions J_2^{p} between pseudo-spins. (d) Another J_2'' is ignored here, because it affects between pseudo-spins.

Compared with the interaction between these pseudo-spins, the in-c-plane NN interactions J_1' between 'real spins' are negligible in the mean-field treatment, because they are canceled out between the zigzag rows, as shown in Fig. 11(a), although the NNN real-spin interactions J_2' [Fig. 11(b)] and J_2'' [Fig. 11(c)] are not. Here, we assume that J_2' and J_2'' are ferromagnetic. The real-spin interactions

J'_2 and J''_2 can be regarded as the NN pseudo-spin interaction J^p_1 and the NNN pseudo-spin interaction J^p_2, respectively. The additional NN real-spin interactions along the zigzag rows only induce the ordering in the pseudo-spins, as shown in Fig. 11(d). Both J^p_1 and J^p_2 must be antiferromagnetic, because J'_2 and J''_2 are ferromagnetic.

Moreover, the NNN pseudo-spin interaction J^p_2 is possibly stronger than the NN pseudo-spin interaction J^p_1, because of the z coordinates of Co ions. As a result, the present pseudo-spin system is considered as the pseudo-spin ANNNI model with NNN interaction stronger than the NN one; however, these two interactions may have similar magnitudes, $J^p_2 \gtrsim J^p_1$. From the present measurements, the ground state of the system is the up-up-down-down structure, which is the same as that of the ANNNI model. This consistency supports the assumption that the NNN real-spin interactions are ferromagnetic.

It is well known that the intermediate phases with various periodicities appear in the ANNNI model. In the present results, the satellite peaks were observed near T_N, and their positions changed with the temperature variation. The satellite peaks might be related to the intermediate phases of the ANNNI model. T_N of TlCoCl$_3$ is determined mostly by the interactions J_0 and J_1. However, J_2 plays a prominent role in the ANNNI-like mechanism. Because J_2 is very weak compared with J_0 and J_1, this mecahnism is valid only in the vicinity of T_N. Therefore, the intermediate phases are expected to be degenerated in a narrow temperature range. Moreover, the $J^p_1 \sim J^p_2$ condition also narrows the temperature range of the intermediate phases. These particular circumstances might induce the peculiar appearance of the satellite peaks. The magnitude of the spin moment of the up-up-down-down structure might be modulated around T_N.

4. Conclusion

To investigate the ordering of the Ising spin on the distorted triangular lattice, the powder and single-crystal neutron diffraction measurements of TlCoCl$_3$ were performed. The crystal symmetries of phases III and V were identified as the $P6_3cm$ and $Pbca$ structures, respectively. At intermediate structural phase IV only the coexistence of the phase III and V reflections was observed. The spin ordering was observed on the zigzag-row lattice. The Ising spins were arranged in an up-up-down-down manner. Immediately above T_N, additional satellite peaks appeared on the shoulder of the $(3/8, 3/8, 1)$ and $(5/8, 5/8, 1)$ magnetic peaks. The spin ordering of Ising spins on the zigzag-row lattice was discussed by considering the ANNNI-like model.

1) M. F. Collins and O. A. Petrenko: Can. J. Phys. **75** (1997) 605.
2) M. L. Plumer, K. Hood and A. Caillé: J. Phys. C **21** (1988) 4189.
3) D. Visser, R. G. Delaplane and W. J. A. Maaskant: Physica B **276–278** (2000) 300.
4) K. Machida, T. Mitsui, T. Kato and K. Iio: Solid State Commun. **91** (1994) 17.
5) D. Visser, G. C. Verschoor and D. J. W. Ijdo: Acta Crystallogr., Sect. B **36** (1980) 28.
6) O. A. Petrenko, M. F. Collins, C. V. Stager, B. F. Collier and Z. Tun: J. Appl. Phys. **79** (1996) 6614.
7) O. A. Petrenko, M. F. Collins, C. V. Stager, B. F. Collier and Z. Tun: Phys. Rev. B **51** (1995) 9015.
8) T. Kato: J. Phys. Soc. Jpn. **71** (2002) 300.
9) K. Yamanaka and T. Kato: J. Phys. Soc. Jpn. **71** (2002) 1757.
10) T. Mitsui, K. Machida, T. Kato and K. Iio: J. Phys. Soc. Jpn. **63** (1994) 839.
11) Y. Nishiwaki, T. Mitsui and K. Iio: J. Phys. Soc. Jpn. **72** (2003) 2608.
12) W.-M. Zhang, W. M. Saslow, M. Gabay and M. Benakli: Phys. Rev. B **48** (1993) 10204.
13) M. Melamud, H. Pinto, J. Makovski and H. Shaked: Phys. Status Solidi B **63** (1974) 699.
14) M. Mekata and K. Adachi: J. Phys. Soc. Jpn. **44** (1978) 806.
15) H. Yoshizawa and K. Hirakawa: J. Phys. Soc. Jpn. **46** (1979) 448.
16) A. Farkas, B. D. Gaulin, Z. Tun and B. Briat: J. Appl. Phys. **69** (1991) 6167.
17) W. B. Yelon, D. E. Cox and M. Eibschütz: Phys. Rev. B **12** (1975) 5007.
18) K. Morishita, N. Nakano, T. Kato, K. Iio and T. Mitsui: Ferroelectrics **217** (1998) 207.
19) K. Morishita, K. Iio, T. Mitsui and T. Kato: J. Magn. Magn. Mater. **226–230** (2001) 579.
20) Y. Nishiwaki, T. Kato, Y. Oohara and K. Iio: J. Phys. Soc. Jpn. **73** (2004) 2841.
21) F. Izumi and T. Ikeda: Mater. Sci. Forum **321–324** (2000) 198.
22) T. Asahi: private communication.
23) R. E. Watson and A. J. Freeman: Acta Crystallogr. **14** (1961) 27.
24) Y. Oohara, M. Mekata, T. Morishita, K. Kakurai, M. Nishi, T. R. Zhao and H. Takei: J. Phys. Soc. Jpn. **70** (2001) 3031.
25) P. Bak and J. von Boehm: Phys. Rev. B **21** (1980) 5297.